Pore network modeling of reaction-diffusion in hierarchical porous particles: the effects of microstructure

Mohammad Amin Sadeghi, Mahmoudreza Aghighi, Jake Barralet, Jeff T. Gostick

PII: S1385-8947(17)31286-X
DOI: http://dx.doi.org/10.1016/j.cej.2017.07.139
Reference: CEJ 17405

To appear in: *Chemical Engineering Journal*

Received Date: 5 April 2017
Revised Date: 17 July 2017
Accepted Date: 23 July 2017

Please cite this article as: M.A. Sadeghi, M. Aghighi, J. Barralet, J.T. Gostick, Pore network modeling of reaction-diffusion in hierarchical porous particles: the effects of microstructure, *Chemical Engineering Journal* (2017), doi: http://dx.doi.org/10.1016/j.cej.2017.07.139

Pore network modeling of reaction-diffusion in hierarchical porous particles: the effects of microstructure

Mohammad Amin Sadeghi[a] – *amin.sadeghi@mail.mcgill.ca*

Mahmoudreza Aghighi[a] – *mahmoudreza.aghighi@mail.mcgill.ca*

Jake Barralet[b, c, d] – *jake.barralet@mcgill.ca*

Jeff T. Gostick[a, d] – *jgostick@uwaterloo.ca*

[a] *Department of Chemical Engineering*, **McGill University**, Wong Building, 3610 University Street, Montreal, Quebec H3A 0C5, Canada

[b] *Faculty of Dentistry*, **McGill University**, Strathcona Anatomy and Dentistry Building, Rue University, Montreal, Quebec H3A 0C7, Canada

[c] *Department of Surgery*, Montreal General Hospital, Faculty of Medicine, **McGill University**, Montreal, Canada

[d] *Department of Chemical Engineering*, **University of Waterloo**, 200 University Avenue West, Waterloo, Ontario N2L 3G1, Canada

Corresponding author at: Department of Chemical Engineering, University of Waterloo, E6-5012, 200 University Ave. W, Waterloo, ON, N2L 3G1. **Email address**: jgostick@uwaterloo.ca

Abstract

A general framework based on pore network modeling is presented for simulation of reactive transport in a porous catalyst with a hierarchy of porosity. The proposed framework is demonstrated in the context of steady state reactive transport inside a nanoporous catalyst particle interlaced with macropores that result from the use of pore-formers. A comprehensive parametric study was performed to examine the influence of structural features namely macroporosity, pore size ratio, and the particle size, as well as transport properties namely pore Damköhler number, on the net reaction rate inside the particle. The results showed that depending on the Damköhler number, increasing the macroporosity does not necessarily improve the catalytic activity of the particle. It was also shown that particles with lower pore size ratios are more kinetically active. The key finding of this work was to demonstrate and quantify how microstructure influences the reactivity of hierarchical porous catalyst particles.

Keywords: hierarchical porous particles; multiscale modeling; pore network modeling; hierarchical network generation; microstructure.

1. Introduction

Porous materials are ubiquitous in nature such as in petroleum reservoirs and biological tissues, and also in engineering applications such as filters, catalyst particles, and electrodes. The pore size and morphology of a porous material strongly influences its transport properties. For instance, a porous material with a unimodal pore size distribution ranging in the nanometer scale provides high surface area yet its transport properties are expected to be weak due to hindered diffusivity in the nanopores. On the other hand, a porous material with a bimodal pore size distribution ranging from micron to nanometer scales would provide better transport properties because the micron-sized pores act as diffusion "highways" throughout the nanometer-scale constrictions. Regular diffusion would occur in the micron-sized pores, while Knudsen diffusion prevails in the nanopores. However, the better diffusivity comes at the price of having less surface area. In the context of catalysis, achieving high surface area and high transport properties simultaneously are two components of an ideal catalyst support; and hierarchical porous materials happen to provide both features. The applications of hierarchical particles include but are not limited to electrochemical energy conversion [1–3], protein adsorption and purification [4,5], supercapacitors [6–9], and tissue scaffolds [10–13]. Although these hierarchical particles are deliberately engineered, there are multiple structural parameters involved in designing a hierarchical material such as macroporosity, pore size ratio, connectivity, so optimization by trial and error is time-consuming and expensive. For this reason, a modelling framework that incorporates the impact of structure on reactive transport in hierarchically porous materials would be a powerful tool for optimal design of catalyst supports for various applications.

Modeling transport in porous materials is a classic and well-established area of research. The proposed models in general can be categorized into two subsets of pore-

scale and volume-averaged continuum models. For brevity, the latter is referred to as continuum models here onwards. Also, note that we use the term pore-scale model only for those models which simultaneously solve transport equations within the porous domain at all length scales. Hence, multi-scale methods with upscaling fall into the category of continuum modeling [14,15]. In continuum models, it is assumed that the porous medium consists of building blocks called representative elementary volumes (REV). REV is the smallest control volume inside a porous domain with physical properties that are representative of the whole [16]. In other words, given that an REV exists, one could replace a porous material with a homogeneous material with equivalent properties. In many simple cases, for example when the structure of the porous material can be approximated by an ordered array of spheres or cylinders, such properties can be calculated analytically. For complex scenarios, however, equivalent properties need to be measured experimentally. While continuum models offer relatively low computational cost, there are two main downsides to this approach. First, they hinge on the fact that an REV exists. However, in certain cases such as in highly anisotropic or very thin materials (e.g. catalyst layer in PEM fuel cells), this is not the case. Secondly, experimental measurements for obtaining effective properties are not always easy to conduct, especially for extremely small porous materials such as nanoparticle agglomerates. This problem escalates for multiphysics problems where different physics such as diffusion, reaction, and heat conduction are intertwined, making it impossible to find reliable constitutive relationships for effective transport properties.

Alternatively, pore-scale models account for the true geometrical heterogeneity of the porous material at the pore scale. They can provide detailed pore-level information even when the material is highly anisotropic or extremely thin. In addition, since the transport equations are solved for the void space within the porous material, there is no

need for measuring equivalent properties as required in continuum models. Instead, bulk fluid properties are used in a pore-scale model, which are widely available in the literature. Capturing pore-level details comes with a price which is higher computational cost. This downside, however, can be mitigated by employing pore network modeling, a less computationally demanding flavor of pore-scale methods. The reason is that since the length-scale of the pores is relatively small, the mixing time-scale becomes extremely short. Therefore, it can be reasonably assumed that the variations of intensive properties such as pressure and concentration within an individual pore is negligible, which significantly reduces the computational cost. Having said that, pore network modeling is the only feasible way to perform a true pore-scale study on hierarchical porous materials. One should be aware that this assumption inevitably introduces some error, but the trade-off enables the study of much larger porous domains for given computational resources. It is worth noting that in traditional continuum models, a notable amount of uncertainty is introduced via volume averaging and experimental error in the determination of the effective properties. Consequently, it is entirely possible that the accuracy of the model is dominated by the uncertainty in volume averaging, rather than the accuracy of the employed numerical scheme for solving the governing equations. Note that pore network modeling was originally meant for multiphase flow where continuum models failed to provide an accurate front-tracking due to structural heterogeneity [17]. The same principles apply to reactive transport problems where structural heterogeneity can potentially cause the results to deviate from what one usually obtains from continuum models. One of the more useful features of pore network modeling is that random structures can be created *in silico*, and the performance of that structure can be determined numerically. The equivalent process with continuum modeling is treating the transport properties as adjustable parameters, but then one has no way of determining which physical configuration of pores and solids leads to a given performance. With pore network

modeling, since structural features such as pore connectivity and tortuosity are built-in, one can physically inspect the network properties as a guide to realizing an actual material.

Modeling transport in hierarchical materials has been conducted using both continuum [14,18–21] and pore-network models [22–24] with emphasis on the former. In the realm of continuum modeling, the common procedure in general is to solve the transport problem at the smallest length scale, and then calculating the bulk properties (e.g. diffusivity) at that scale by means of volume-averaging, and repeating this process until reaching the largest length scale [21]. This approach has both upsides and downsides which were critically discussed above. Although pore network modeling is a powerful tool for studying transport in hierarchical materials, most of the available works in this area date back almost two decades, such as the works of Meyers and Liapis [23,24], and Petropoulos et al. [22]. Petropoulos et al. (1991) set the groundwork for studying transport in hierarchical materials [22], however, the size of the network they chose, presumably due to limited processing power, was not large enough to entail the interesting interactions between structural features and transport properties. Moreover, the hierarchical network they proposed is an ordered cubic network (i.e. macropores) mapped onto a finer network (i.e. nanopores) rather than a true hierarchical network. In addition, they did not study the influence of different structural parameters on transport properties. Some years later, Meyers and Liapis (1998, 1999) extended the framework developed by Petropoulos et al. to incorporate reactive transport with advection in hierarchical materials in the context of an adsorption column [23,24]. Although interesting, their work lacks generality and is limited to studying the influence of pore connectivity and fractional saturation of active reaction sites on bulk properties such as intraparticle interstitial fluid velocity. Hence, their work does not

provide a clear picture of the interplay between structural features of hierarchical materials and transport properties.

The objective of the present study is to extend previous attempts and to formulate a general yet easy-to-use modelling framework for simulating reactive transport in hierarchical porous materials. Furthermore, an extensive study on the interplay between structural features and transport properties in the context of hierarchical materials is missing in the literature and in this respect, this study is an attempt to fill this gap. The present analysis is performed on a hierarchically porous particle with a bidisperse pore size distribution, such as nanoporous particle interlaced with macropores that resulting from the use of porogens or pore-formers. The numerical recipe introduced in the present work can be used to estimate performance in terms of net reaction rate of an arbitrary hierarchical porous particle with certain structural features such as pore/throat size distribution given as the model inputs, to come up with optimal designs for applications of interest.

2. Model development

2.1. Pore network modeling

Pore network modeling is a pore-scale method for studying transport phenomena and fluid flow in porous media. In this approach, the porous domain is mapped onto a set of pores (i.e. void spaces) connected through throats (i.e. constrictions in the void space). How well a pore network model represents a realistic particle depends on how faithfully the model geometry matches the network structure. It is possible to extract networks from tomography images of the porous material [25–28], but this is not feasible for nanoscale and hierarchical materials due to resolution limitations, and moreover, network extraction algorithms are not trivial [29–32]. Fortunately, it has been shown that randomly generated networks can be calibrated such that they show

equivalent static and dynamic properties such as pore/throat size distribution and percolation threshold, compared to those of the actual network [17,33,34]. The calibration can be done by performing different simulations such as capillary drainage, gas diffusion, and permeability [35,36], and adjusting the network geometry until all experimental data is simultaneously matched. The aim of the present work is to facilitate designing hierarchical catalyst supports, so instead of matching existing materials, new structures are explored and analyzed. To this end, hierarchical particles with certain structural features as tunable parameters are realized *in silico*. Then, by performing a parametric study on the tunable parameters, performance curves in terms of net reaction rate within the particle are obtained, which can finally be used as guidelines for designing actual catalyst supports. All the computer implementation of this study was performed using OpenPNM, which is an open-source software in Python for simulation of transport and fluid flow in porous media [37].

2.2. Generating hierarchical networks

In this work two methods for generating networks with a hierarchy of porosity are proposed, namely top-down and bottom-up. The bottom-up approach, as shown in Figure 1a, begins with a cubic network that consists only of nanopores with an arbitrary pore size distribution. To create macropores, a random nanopore and all its nearby nanopores within a certain distance r_m are chosen. These pores are then removed from the network and replaced with a single macropore. By repeating this process, arbitrary hierarchical porous structures with increasing macroporosity can be achieved. Macroporosity ϕ_m is defined as

$$\phi_m = \left(1 - \frac{\mathrm{N_{np}}}{\mathrm{N_{n,i}}}\right) \times 100 \qquad (1)$$

where N_{np} is the number of nanopores, and $N_{n,i}$ is the number of nanopores in the initial nanoporous network. In the Top-down approach, as shown in Figure 1b, we start with a cubic network that consists entirely of macropores. Next, we consecutively select a random pore and replace it with a finer network that consists of only nanopores. By repeating this process, arbitrary hierarchical porous structures with decreasing macroporosity can be obtained. The top-down approach is used in this work since this represents the physical process by which nanoporous particles with pore-forming additives are generated. A summary of the networks generated in this study is presented in Table 2.

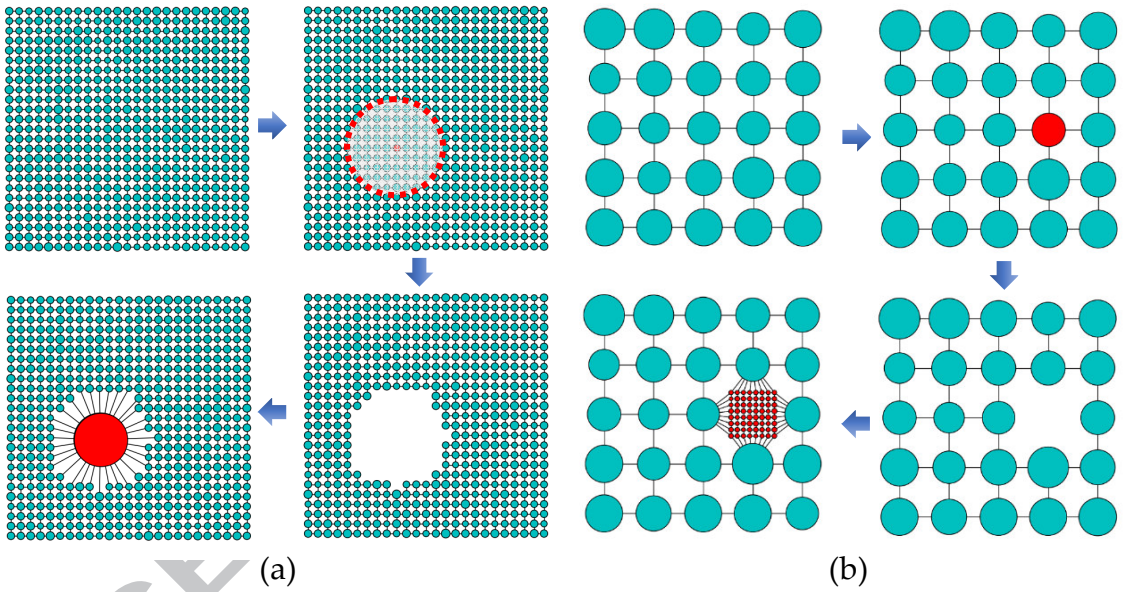

Figure 1- (a) Bottom-up approach for generating hierarchical pore networks: (1) generating the initial network, containing nanopores only (top left), (2) randomly selecting a pore and finding its nearby pores within a certain distance (top right), (3) removing the pores that satisfy the condition from the network (bottom right), and finally (4) inserting the largest macropore that fits in the created empty space (bottom left). (b) Top-down approach for generating hierarchical pore networks. (1) generating the initial network, containing macropores only (top left), (2) randomly selecting a pore (top right), and (3) removing it from the network (bottom right), (4) and finally replacing the removed pore with a finer network (bottom left).

Table 1- Summary of some of the generated networks in this study

d_p (μm)	r_m (nm)	ϕ_m (%)	N_{np}	N_{mp}

40	1,000	15	106,760	60
40	1,000	50	62,800	200
40	500	50	62,800	800
20	1000	15	26,690	15
20	500	35	20,410	140
10	500	20	6280	20
10	200	75	1963	468

Note that the pore/throat size (diameter) distributions of the nanoporous networks used in either of the two strategies were set according to a Gaussian distribution as shown in Figure 2. The spacing of the nanoporous networks was 100 nm. Spacing in a cubic network is defined as the center-to-center distance of two arbitrary neighbor pores. The center-to-center distance between two macropores varies randomly between R and $2R$ due to the bottom-up construction process, which selected macropore centers at random from existing nanopores. These nanopores are always more greater than R from the nearest macropore, and macropores only connect to each other if they are with $2R$. The throat length distribution can be readily calculated once the pore size distribution is established. The present study is focused on 2d networks and therefore, surface areas and volumes are calculated accordingly, i.e., throat and pore cross-section areas become their diameters, available reaction area within a pore becomes its circumference, and finally total particle volume becomes its surface area.

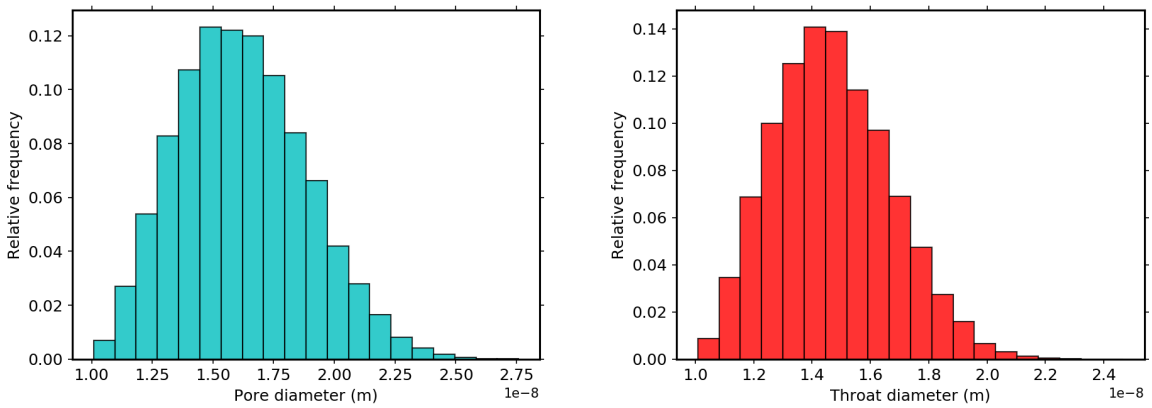

Figure 2- Pore/throat size distribution of the nanoporous networks used in the present study.

We used an Intel® Xeon® CPU E5-1650 v3 @ 3.50 GHz computer with 16 GB of memory for network generation and transport simulations. The transport simulation runtime for even a 3d network consisting of 1 million pores was less than a minute. However, the network generation was very slow since the calculations are serial in nature. Since we wanted to perform several parametric studies, we decided to perform the simulations in 2d rather than 3d.

2.3. Mathematical formulation

Once the network topology and physical properties are set, it is possible to model transport processes occurring through the network. A steady-state mass balance around pore i in the network gives

$$-\sum_{k=1}^{N_i} m_{ik} S_{ik} + R_i = 0 \qquad i = 1,2,\dots,N_p \qquad (2)$$

where N_i is the number of neighboring pores, N_p is the total number of pores in the network, m_{ik} is the mass flux from node i to k, S_{ik} is the cross-section area of the connecting throat, and R_i is the net reaction within pore i. In this study, it was assumed

that nanopores are entirely covered with catalyst. Here, because of the small length scale of the nanoporous particle, advection is assumed to be negligible. Hence, m_{ik} only consists of molecular diffusion and is

$$m_{ik} = -D_e \frac{c_k - c_i}{\ell_{ik}} \tag{3}$$

where D_e is the effective diffusivity in throats and is composed of Knudsen and bulk diffusion, and ℓ_{ik} is the length of the connecting throat between pore i and k. For the reaction term, it was assumed that reaction sites are only present in nanopores. This assumption is valid since macropores do not significantly contribute to the total surface area. For this study, first order reaction kinetics were assumed

$$R_i = -kA_i c_i \qquad i = 1,2,\dots,\mathrm{N_{np}} \tag{4}$$

where k is the rate constant per unit area, A_i is the internal surface area of pore i. In case of a nonlinear reaction kinetics, nothing changes except the system of equations need to be solved iteratively.

2.3.1. Knudsen diffusion

When the pore diameter in a porous structure is comparable to the mean free path of the enclosed molecules, molecular diffusion gets hindered by frequent collisions with the pore wall, otherwise known as Knudsen diffusion. The Knudsen diffusivity can be calculated from

$$D_{KA} = \frac{d_p}{3}\sqrt{\frac{8R_g T}{\pi M_A}} \tag{5}$$

where d_p is the pore diameter, R_g is the universal gas constant, T is the system temperature, and M_A is the molecular weight of species A. The relation for Knudsen

diffusivity can be derived from the self-diffusion coefficient from the kinetic theory of gases [38]. Since the diffusive resistances due to binary and Knudsen diffusion are in parallel, the effective diffusivity of species A in a binary mixture containing A and B can be calculated from

$$\frac{1}{D_{Ae}} = \frac{1}{D_{AB}} + \frac{1}{D_{KA}} \tag{6}$$

where D_{Ae} is the effective diffusivity of A in the mixture, D_{AB} is the binary diffusivity of A, and D_{KA} is the Knudsen diffusivity. The values of the parameters used in Eq. (1) to (6) are listed in Table 2.

Table 2- Parameters used in this study

Parameter	Value	Unit	Description
$\boldsymbol{\phi_m}$	-	-	Macroporosity
$\boldsymbol{N_{np}}$	-	-	Number of nanopores in the hierarchical network
$\boldsymbol{N_{n,i}}$	-	-	Number of nanopores in the initial network
$\boldsymbol{m_{ik}}$	-	$kg/m^2.s$	Mass flux from pore i to k
$\boldsymbol{S_{ik}}$	-	m^2	Cross-section area of the throat between pore i and k
$\boldsymbol{\ell_{ik}}$	-	m	Length of the throat between pore i and k
$\boldsymbol{R_i}$	-	kg/s	Reaction rate in pore i
$\boldsymbol{k}$	-	m/s	First order reaction rate constant
$\boldsymbol{A_i}$	-	m^2	Active reaction area of pore i
$\boldsymbol{c_i}$	-	kg/m^3	Concentration of species in pore i
$\boldsymbol{d_p}$	-	m	Pore diameter
$\boldsymbol{R_g}$	8.314	$J/mol.K$	Universal gas constant
$\boldsymbol{T}$	298.15	K	Temperature
$\boldsymbol{M_A}$	16	$kg/kmol$	Molecular weight of the species
$\boldsymbol{D_{AB}}$	0.176	cm^2/s	Bulk diffusion coefficient of the species
$\boldsymbol{D_{KA}}$	-	cm^2/s	Knudsen diffusion coefficient of the species
$\boldsymbol{D_{Ae}}$	-	cm^2/s	Effective diffusion coefficient of the species

2.3.2. Boundary conditions

The proposed mathematical model for a hierarchical nanoporous particle as shown in Figure 3 was numerically solved under steady state conditions and with first order reaction in nanopores, and constant concentration $c_A = 1\,\mathrm{mol/m^3}$ for the external boundary pores.

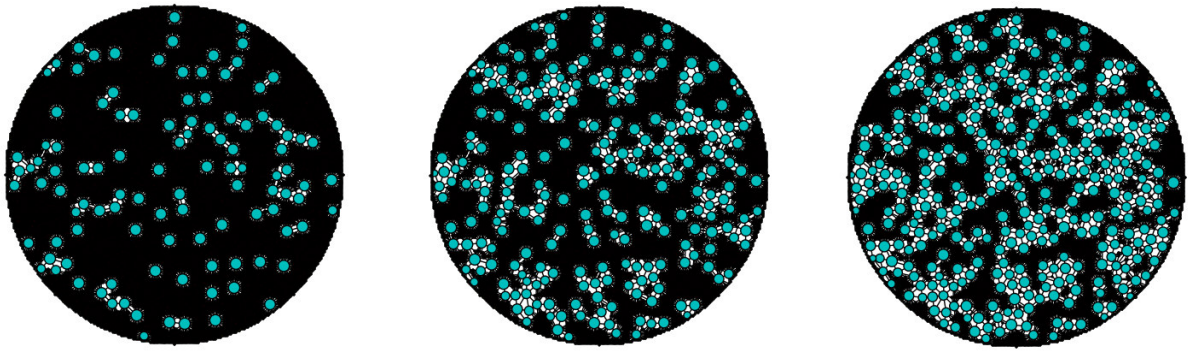

Figure 3- Schematic of the hierarchical nanoporous particles at three different macroporosity $\phi_m = 25\%, 50\%,$ and 67% (left to right). Blue/black circles refer to macropores/nanopores.

3. Results and discussion

The results of this study are presented in the format of a parametric sweep of a variety of physical properties of particles to understand the effects of different structures on the net reaction rate within the nanoparticle. The aim is to determine a recipe for a particle that provides the highest reaction rates with the smallest amount of catalyst material. Since network are generated randomly and subject to variability, each simulation was repeated five times with different random seed numbers. For this reason, most of the figures include error bars indicating two standard deviations. Figure 4 shows typical results obtained from these simulations. In this figure, concentration contours (units are $\mathrm{mol/m^3}$) are illustrated for four hierarchical particles with different macroporosities. For

clarity, macropores are shown as void spaces. Note that the color bars have different scales, so the particle with 58% macroporosity shows a more uniform concentration distribution than the others. This reason for this is that the macro pores facilitate transport into the center of the particle, which will be analyzed in depth in a subsequent section.

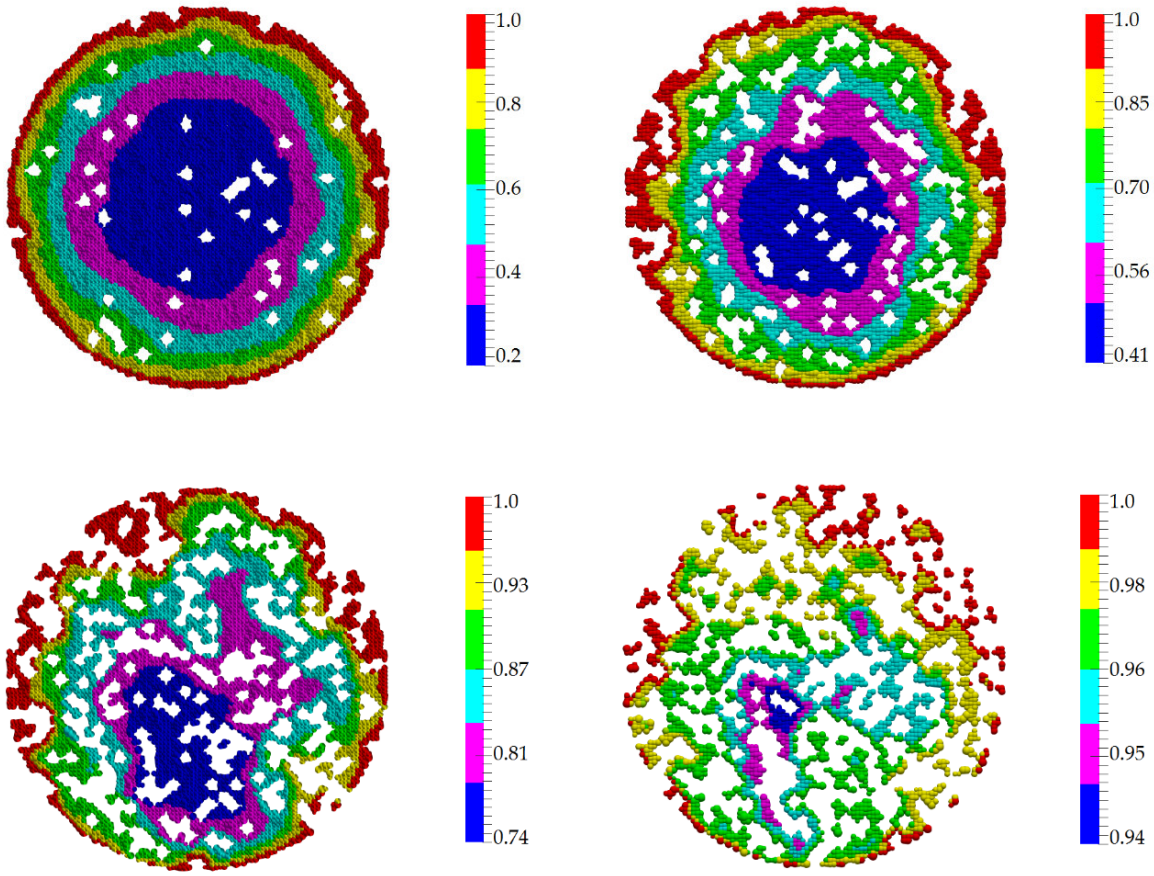

Figure 4- Concentration contours of four hierarchical porous particles (d = with macroporosities ϕ_m of 8% (top-left), 25% (top-right), 41% (bottom-left), and 58% (bottom-right). Void spaces refer to the macropores.

3.1. Influence of macroporosity

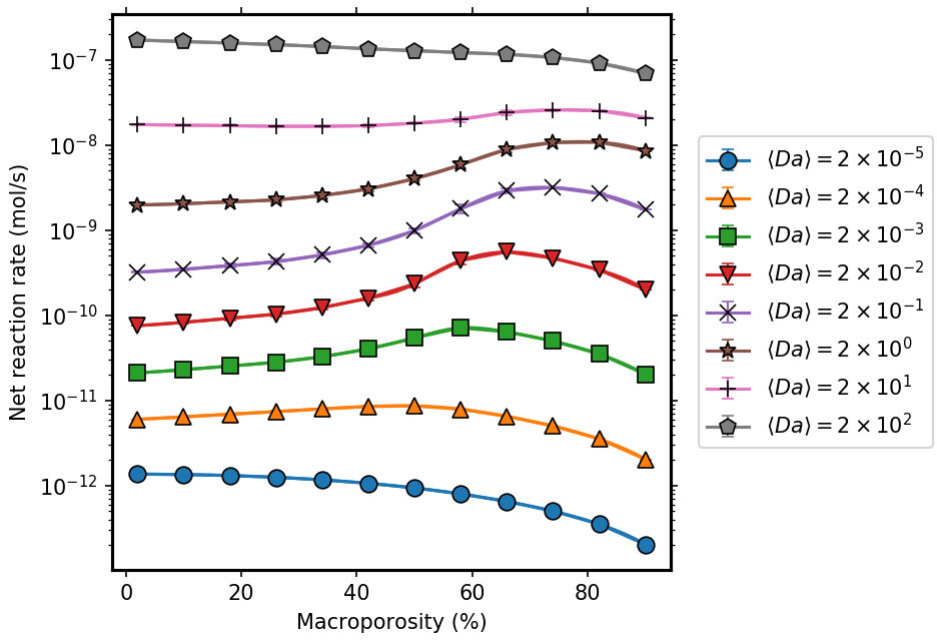

Figure 5- Net reaction rate vs. macroporosity at different average pore Damköhler numbers; $R_p = 20\ \mu m$, PSR= 20.

Figure 5 shows the net reaction rate versus macroporosity at different average pore Damköhler numbers for a particle with a radius of 20 μm and an average pore size ratio of 20. Pore size ratio is defined as the ratio of the average diameter of macropores to that of nanopores. The average pore Damköhler number $\langle Da \rangle$ is defined as the average of local Damköhler numbers in nanopores. The local Damköhler number is the ratio of reaction rate constant within a pore kA_i to sum of the diffusive conductance of its neighboring throats. Thus, average pore Damköhler number can be expressed as

$$\langle Da \rangle = \left[\frac{kA_i}{\sum_k DS_{ik}/\ell_{ik}} \right] \qquad i = 1,2,\dots,\mathrm{N_p} \qquad (7)$$

Based on Figure 5, two distinct trends for the net reaction rate can be observed as the macroporosity increases: in some cases the reaction rate monotonically decreases, and in other cases, it shows a maximum at some intermediate macroporosity. As the

macroporosity increases, less reaction sites are available and thus the net reaction rate is expected to decrease. However, at higher macroporosities more diffusion highways (i.e. macropores) are available which provide enhanced transport of species. Hence, by increasing the macroporosity the net reaction rate does not necessarily increase or decrease, but depend on other structural factors.

The trends that are shown in Figure 5 can be explained by considering the average pore Damköhler number. As defined in the previous sections, average pore Damköhler number is a measure of relative strength of reactivity to diffusivity of species inside individual pores. At relatively low average pore Damköhler numbers ($\mathrm{Da} \approx 10^{-6}$), diffusivity of species is far superior to their reactivity. Therefore, increasing the macroporosity does little to help the transport of the diffusing species, and also decreases the number of available reaction sites. Under these circumstances, it is expected that the net reaction rate monotonically decreases by increasing the macroporosity. At moderate average pore Damköhler number ($\mathrm{Da} \approx 10^{-4}$ to 1.0), diffusivity of species starts to decline and therefore the inner core of the particle gradually becomes underutilized. Under such conditions, creating macropores within the particle improves the diffusivity and helps reactant penetrate deeper into the particle, causing the net reaction rate to increase. Even though some of the reaction sites are removed, the resulting boost in diffusivity compensates for the loss of reactive surface area. Nevertheless, by further increasing the macroporosity the subsequent enhanced diffusion cannot anymore compensate for the loss of reactive surface area, causing the net reaction rate to decrease. Finally, at relatively high average pore Damköhler numbers ($\mathrm{Da} \approx 10^{2}$), diffusivity of species is significantly limited compared to their reactivity. Consequently, the diffusing species is rapidly consumed at the surface pores, leading to a complete starvation of the internal pores within the porous network. Under these circumstances, one might expect that increasing the

macroporosity facilitates the diffusing species to reach the innermost regions as well. However, this is not the case since the diffusivity of species is significantly hindered such that the subsequent boost in diffusivity as a result of creating macropores cannot account for the loss of reactive surface area. Consequently, net reaction rate is monotonically decreased by increasing macroporosity. Note that macroporosities above 90% were not investigated since such a physical particle is likely to fall apart, while the active surface area decreases dramatically, which is not desirable.

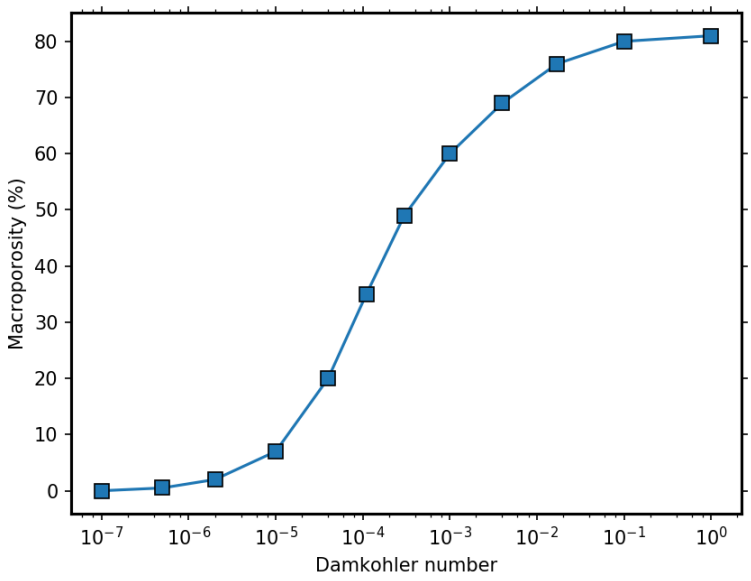

Figure 6- Locus of maximum reaction rates vs. average pore Damköhler number; $R_p = 20\ \mu m$, PSR= 20.

Figure 6 displays the locus of maximum net reaction rates (in terms of macroporosity) against the average pore Damköhler number for particles with a radius of 20 µm and a pore size ratio of 20. Following the discussions above, at relatively low average pore Damköhler numbers since the diffusivity is superior to the reactivity, increasing the macroporosity only reduces the number of available reaction sites, causing the net reaction rate to monotonically decrease. Hence, the maximum net reaction rate is expected to occur at relatively low macroporosities (i.e. $\epsilon_m \approx 0$). At moderate pore

Damköhler numbers, by increasing macroporosity, initially the net reaction rate increases due to the subsequent boost in diffusivity, and then declines since the loss of reactive surface area becomes the limiting factor. In this regime, the macroporosity at which the net reaction rate within the particle is maximized entirely depends on the average pore Damköhler number. As the average pore Damköhler number increases, the diffusivity of species is continually hindered. Therefore, to reach the potential maximum net reaction rate, the particle needs to be more macroporous in order to facilitate the species to penetrate deep down the particle, which causes the locus of maximum net reaction rate to shift towards higher macroporosities. Finally, at relatively high average pore Damköhler numbers (not show in Figure 6), the reactivity of species is much superior than their diffusivity such that the improved diffusivity from creating macropores cannot compensate for the resulting loss of reactive surface area, causing the net reaction rate to continually decrease. Thus, the maximum net reaction rate occurs at relatively low macroporosities (i.e. $\epsilon_m \approx 0$).

3.2. Influence of pore size ratio

Figure 7 shows the net reaction rate against macroporosity at different pore size ratios for a particle with a radius of 10 μm and an average pore Damköhler number of 7×10^{-2}. For a given macroporosity the particle with the lowest pore size ratio is the most reactive. This outcome is rather counterintuitive since a higher pore size ratio leads to formation of larger diffusion highways and consequently better transport of species. Therefore, it is expected that particles with higher pore size ratio should be more reactive. The observed effect can be explained by inspecting the structure of the particles with different pore size ratios.

Figure 8 illustrates the structure of three identical particles 40% macroporosity except each was constructed at a different pore size ratio. When the pore size ratio is relatively high although the diffusion highways (i.e. the macropores) are larger, they are not well-

dispersed within the particle and they mostly appear isolated blobs within the nanoporous matrix. Hence, the subsequent diffusion enhancement because of the presence of macropores is minimal.

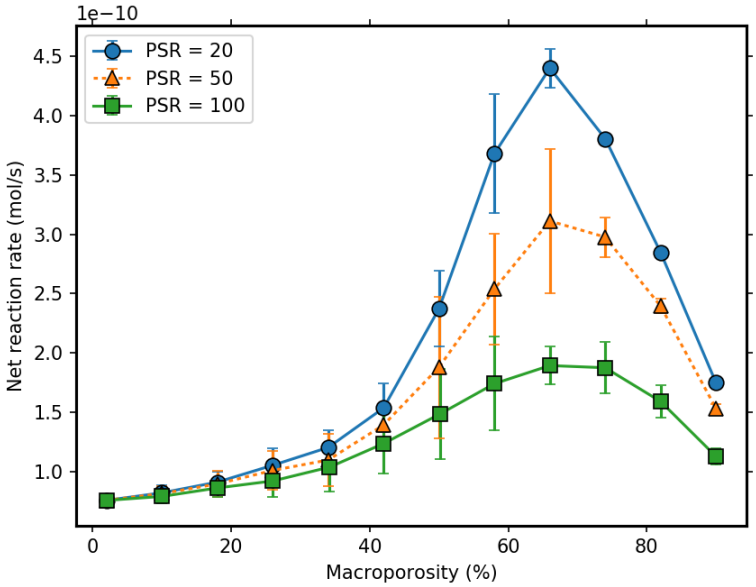

Figure 7- Net reaction rate vs. macroporosity at different pore size ratios; $R_p = 10\ \mu m$, $\langle Da \rangle = 0.07$.

On the other hand, when the pore size ratio is relatively low the macropores are well-dispersed throughout the nanoporous matrix and therefore provide the diffusing species with decent accessibility to reach the innermost regions of the particle. One could argue based on percolation theory, that pore connectivity in 2d is much worse than that in 3d. Therefore, the significant difference in net reaction rates observed for different pore size ratios might be an artifact of the ill-connected macropores in our 2d simulation. While this behavior is important for fluid percolation simulations, it is less relevant for diffusive transport. The reason is that in a fluid percolation simulation, either a pore is invaded or not, whereas in diffusive transport, diffusion transpires seamlessly no matter how small the diffusive conductance is. Moreover, the advective flux between two pores is roughly proportional to d_p^3 whereas the diffusive flux is

proportional to d_p, assuming the throat diameter and throat length are of the same order of magnitude. Consequently, isolated nanopores in a flow problem are much more likely to have virtually no contribution to the overall transport. In other words, in flow problems the worse connectivity in a 2d representation might lead to inaccurately neglecting the contribution of those isolated nanopores that otherwise in a 3d representation would have access to a nearby macropore and therefore contribute to the overall transport. Having said that, the worse connectivity in 2d is unlikely to qualitatively change the behavior observed in the simulations, but rather quantitatively.

One direct outcome of above explanation is that at higher pore size ratios, because macropores are not well-dispersed within the particle, the average distance between a nanopore and the nearest macropore is relatively higher, which leads to reactant starvation at such nanopores. Consequently, the net reaction rate decreases. On the other hand, at lower pore size ratios, reactant starvation is less frequent since macropores are well-dispersed within particle and therefore the average distance between an arbitrary nanopore to the nearest macropore is shorter, increasing the net reaction rate.

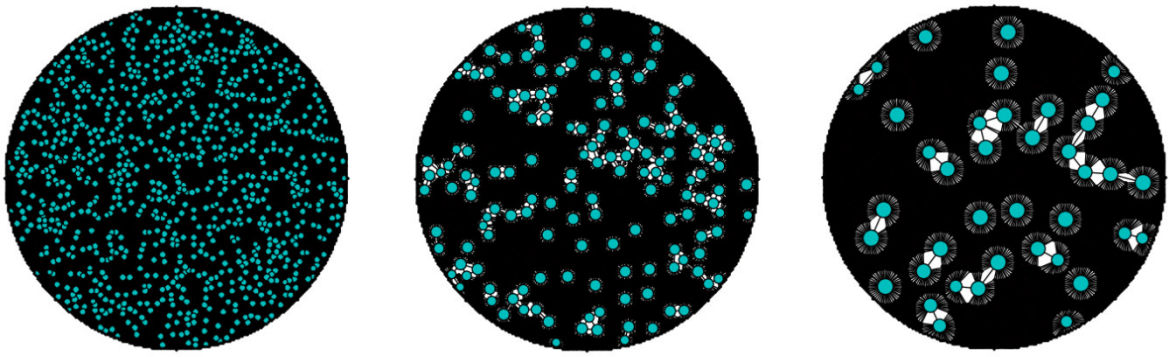

PSR = 20 *PSR* = 50 *PSR* = 100

Figure 8- Microstructure of particles at different pore size ratios; $R_p = 10\ \mu m$, $\phi_m = 40\%$

Figure 9 shows the histogram of reaction rates in the nanopores for a particle at two different pore size ratios of 20 and 100, along with the ideal case where effective diffusivity in the particle is infinity (such that the presence of macropores is irrelevant to transport). Also, cumulative reaction rates for each scenario are plotted. Based on this figure, the histogram for $PSR = 100$ is shifted towards lower reaction rates, with indicates that that nanopores are operating at lower concentrations, therefore decreasing the net reaction rate within the particle. On the other hand, the histogram for $PSR = 20$ is shifted towards higher concentrations, implying that nanopores are operating at relatively higher concentrations, therefore increasing the net reaction rate within the particle.

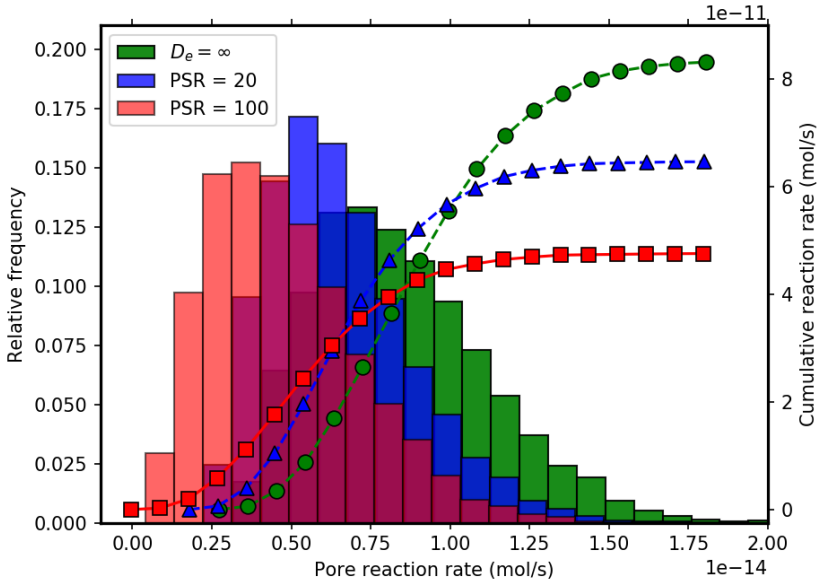

Figure 9- Histogram of reaction rates in nanopores. Lines are cumulative reaction rate; $R_p = 10\ \mu m$, $\langle Da \rangle = 0.07$ ϕ_m= 66%

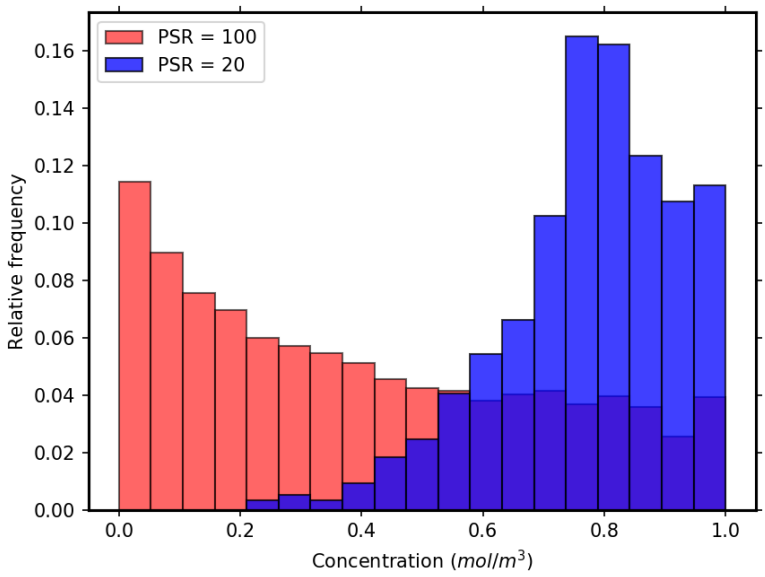

Figure 10- Histogram of concentration in nanopores; $R_p = 10\ \mu m$, $\langle Da \rangle = 0.07$, ϕ_m= 66%

This pore-by-pore analysis of reaction rates and local concentrations is a specific benefit of pore-scale modeling. In this case, it reveals very clearly that large sections of the particle are performing poorly because they are essentially starved of reactant by their lack of proximity to a macropore. This claim is better understood and confirmed by looking at the concentration histogram/contour in nanopores, shown in Figure 10 and Figure 11. Figure 10 shows the histogram of nanopore concentration for two identical hierarchical particles with different pore size ratios.

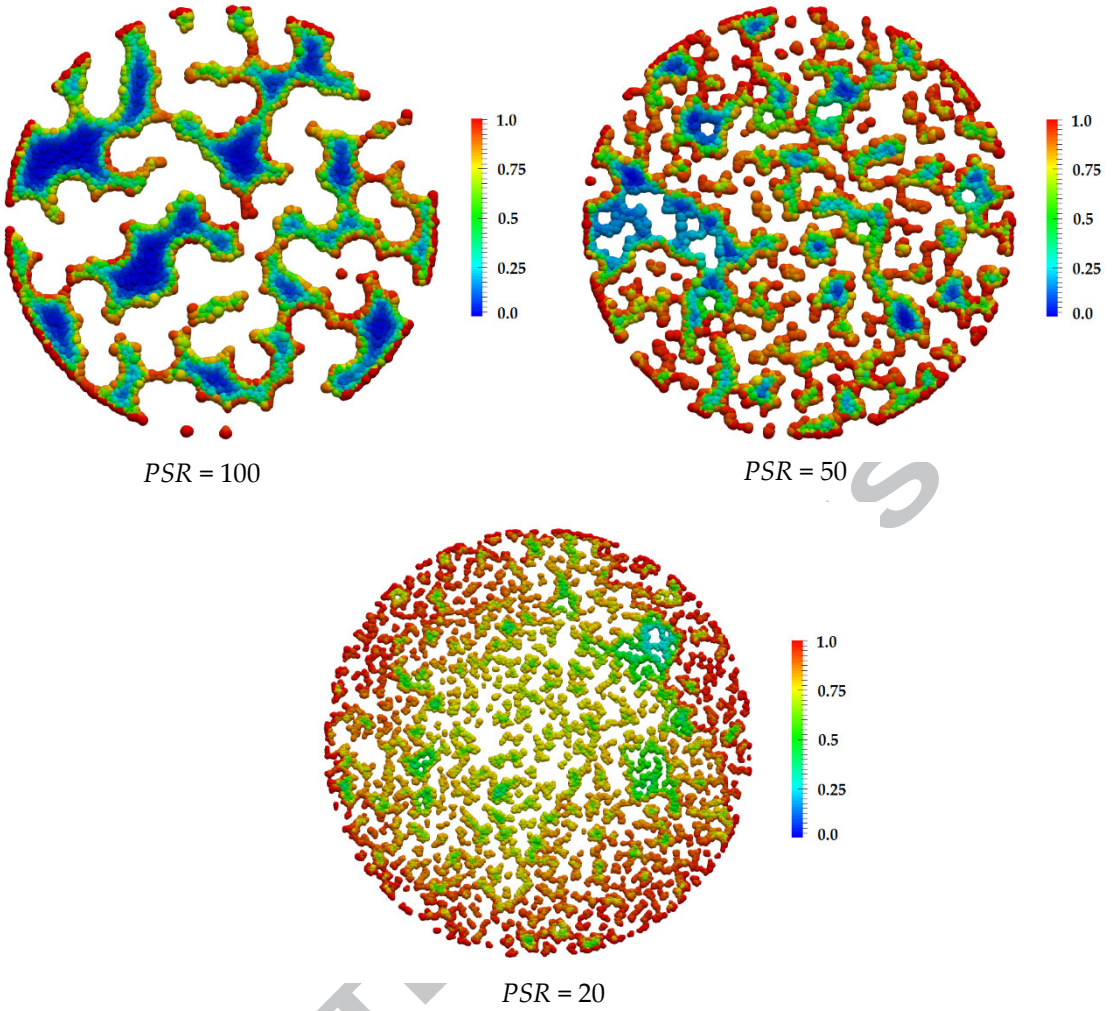

Figure 11- Concentration contour in nanopores (units are mol/m^3); $R_p = 10\ \mu m$, $\langle Da \rangle = 0.07$, ϕ_m= 66%

According to the histogram plot, almost all the nanopores in the particle with $PSR = 20$ are operating at concentrations greater than $0.5\ mol/m^3$. On the other hand, a substantial portion of the nanopores in the particle with $PSR = 100$ are starving of reactant, working at concentrations below $0.5\ mol/m^3$. The concentration contour plots shown in Figure 11 confirm such behavior. According to the contour plots, it is clearly observed that for the particle with the largest pore size ratio ($PSR = 100$), the nanopores which are not in the proximity of a macropore are starved of reactant. However, this is not the case for the particle with the lowest pore size ratio ($PSR = 20$) since a larger

fraction of the nanopores are close to at least one macropore, providing them with sufficient amounts of reactant.

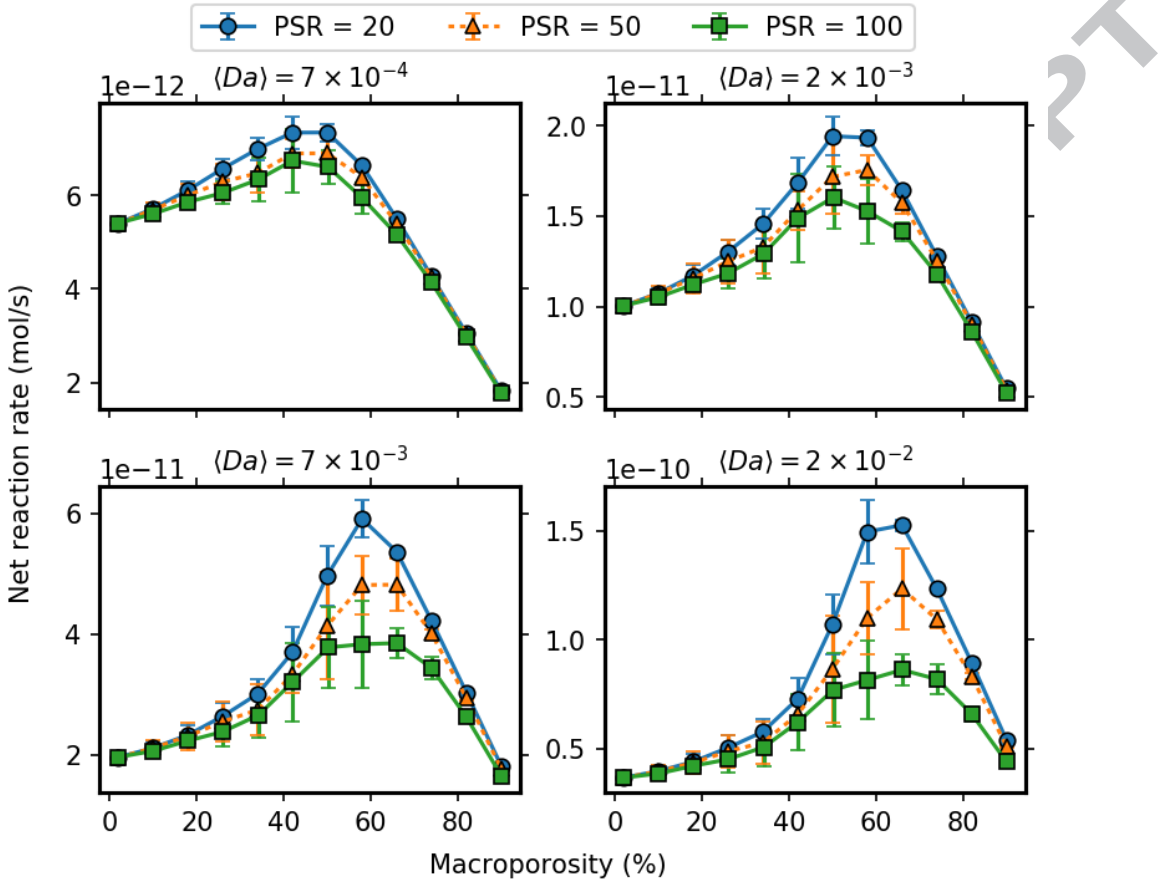

Figure 12- Net reaction rate vs. macroporosity at different pore size ratios and pore Damköhler numbers; $R_p = 10\ \mu m$

Figure 12 is the same as Figure 7 except plotted at different average pore Damköhler numbers. Based on Figure 12, the average pore Damköhler number can significantly attenuate the effect of pore size ratio on the reactivity of the particle. At relatively high average pore Damköhler numbers ($\langle Da \rangle \approx 0.01$) since diffusion is very limited, particles can benefit from the enhanced diffusion due to the lower pore size ratio. On the contrary, when the average pore Damköhler number is relatively small ($\langle Da \rangle \approx 10^{-4}$), diffusion is already at its maximum state. Accordingly, varying the pore size ratio has

minimal effect on the diffusivity, therefore particles with different pore size ratio approximately show the same performance.

It noteworthy that merely by playing with the structure, the particle with $PSR = 20$ at about 66% macroporosity has almost achieved 350% increase in the net reaction rate compared to a nonhierarchical nanoporous particle. While 350% improvement is a poor increase compared to what potentially can be achieved by playing with the kinetics of the reaction (see Figure 5), kinetics is usually not considered a manipulating parameter and is rather forced by the reaction/catalyst. However, structure can be more easily manipulated to obtain highly reactive particles.

Figure 13 illustrates how particle size influences the effect of pore size ratio on the net reaction rate. Based on this figure, when the particle is relatively small, those with different pore size ratios show nearly identical performances, while for relatively big particles, the performance of those with different pore size ratios differ. The reason is that at relatively small particle sizes diffusion is not the limiting mechanism and therefore, the boosting effect of pore size ratio on diffusivity, which was discussed above in detail, becomes irrelevant. As the particle size increases, reactant diffusion gradually gets hindered and consequently, the boosting effect of pore size ratio becomes significant, causing particles with different pore size ratios to show different performance curves.

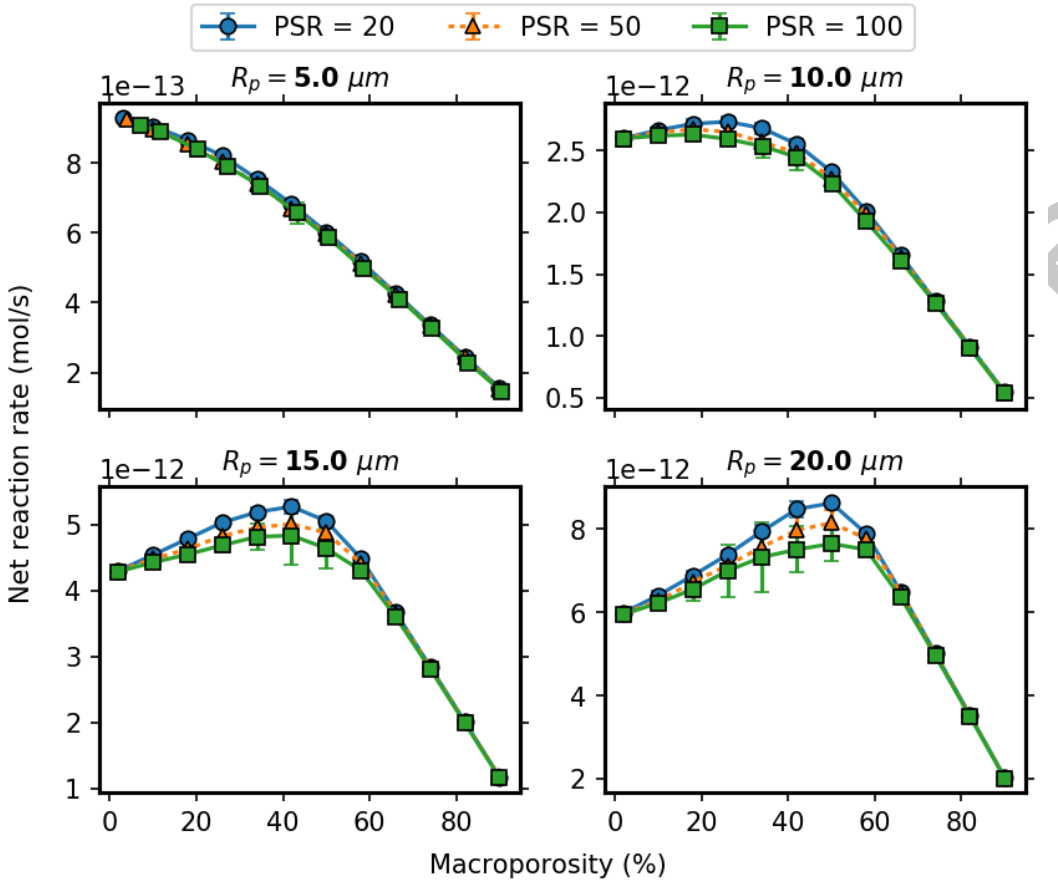

Figure 13- Net reaction rate vs. macroporosity at different pore size ratios and particle sizes; $\langle Da \rangle = 2 \times 10^{-4}$

3.3. Analysis of particle utilization

One of the performance metrics that can be used to analyze the efficiency of the particles is net reaction rate normalized with respect to their bulk volume. Such analysis is beneficial for certain applications such packed bed reactors where total volume is fixed. Figure 14 illustrates the effect of particle size on the reactivity of the particles. The y-axis shows the net reaction rate normalized by the volume of the particle V_p defined as

$$V_p = \pi R_p^2 \times 1 \tag{8}$$

where R_p is the radius of the particle. Note that since we are performing 2d simulations, the volume of the particle is its surface area, which should be multiplied by 1 meters depth to account for the correct dimension. Each curve represents a particle with a particular radius. Based on this figure, the particles with smaller radius are favorable in terms of net reaction rate per unit volume. This observation can be explained by the fact that for the case of larger particles, a large portion of the diffusing species gets consumed near the surface of the particle. Hence, many reaction sites in the innermost regions of the particle are unused. Therefore, it is expected for the smaller particles to be more kinetically-active.

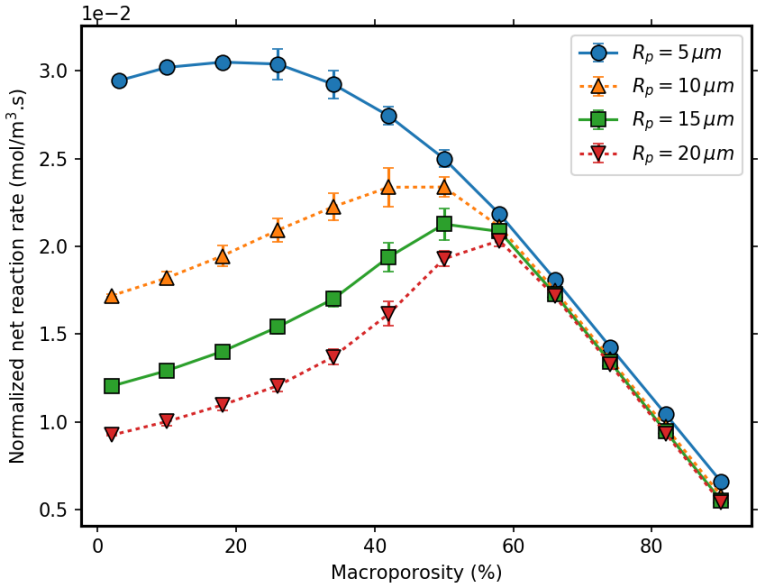

Figure 14- Normalized net reaction rate vs. macroporosity at different particle size; $\langle Da \rangle = 7 \times 10^{-4}$, *PSR*= 10

Another interesting feature of Figure 14 is the locus of maximum net reaction rate. Based on this figure, as the particle size increases, the macroporosity at which the particle is most reactive increases as well. For instance, a particle with a radius of 5 μm is most reactive at around 10% macroporosity whereas a particle with a radius of 20 μm is most reactive when the macroporosity is about 60%. Having said that, creating a

hierarchy of porosity is not always favorable. In fact, larger particles tend to be more reactive at high macroporosities while smaller particles are most reactive when there is no hierarchy of porosity present. This is of course because in small particles all reaction sites are generally near the surface concentration, which is the situation being emulated by the addition of macroporosity in larger particles.

4. Conclusion

In this work, a general framework based on pore-network modeling was developed to study reactive transport within a single 2d porous particle with a hierarchy of porosity at steady state conditions. A parametric study of particle physical properties was performed to capture the effects of pore structure on the performance of the particle in terms of net reaction rate. These parameters include particle size, average pore size, macro to nano pore size ratio, and average pore Damköhler number. The results showed that as macroporosity increases, depending on the average pore Damköhler number, two distinct trends can be observed for the net reaction rate: monotonic decrease, and mixed behavior. In addition, it was shown that at a constant macroporosity, the particle with a lower pore size ratio is more reactive. The results of this can be used as a guideline to design hierarchical catalysts supports that are more reactive due to their optimal structure. Note that, however, a single recipe cannot be realized for making more reactive particles since the reaction kinetics plays an important role. Hence, depending on the reaction kinetics of the system, the optimum structure for the catalyst particle to be most reactive could vary from being entirely nanoporous to mostly macroporous.

Future work should include modeling 3d particles to provide more realistic connectivity which was found to be a key factor in this work. Because of the 2d limitation of the present work, these reported trend are qualitatively only, although we

expect the trends to hold for 3d particles. Also, for multicomponent systems it is more rigorous to employ Maxwell-Stefan theory for diffusion calculations. The present approach is completely agnostic to the network dimensionality, but computational requirements grow very quickly. Also along the lines of more realistic simulations, it would be quite relevant to include heat evolution from the reaction and heat transfer out of the particle, as this would impact the local kinetics. In the context of this work, the existence of macropores in the particle allow faster gas diffusion, but will hinder heat conduction and reduce heat capacity. Truly optimizing a particle requires coupling multiple physics.

Acknowledgment

The authors would like to express their gratitude to the Natural Science and Engineering Research Council (NSERC) of Canada, as well as Ballard Power Systems for providing financial support throughout the course of this project.

References

[1] P. Trogadas, V. Ramani, P. Strasser, T.F. Fuller, M.-O. Coppens, Hierarchically Structured Nanomaterials for Electrochemical Energy Conversion, Angew. Chemie Int. Ed. 55 (2016) 122–148. doi:10.1002/anie.201506394.

[2] A. Magasinski, P. Dixon, B. Hertzberg, A. Kvit, J. Ayala, G. Yushin, High-performance lithium-ion anodes using a hierarchical bottom-up approach., Nat. Mater. 9 (2010) 353–358. doi:10.1038/nmat2749.

[3] F. Cheng, J. Liang, Z. Tao, J. Chen, Functional Materials for Rechargeable Batteries, Adv. Mater. 23 (2011) 1695–1715. doi:10.1002/adma.201003587.

[4] Q. Fu, X. Wang, Y. Si, L. Liu, J. Yu, B. Ding, Scalable Fabrication of Electrospun

Nanofibrous Membranes Functionalized with Citric Acid for High-Performance Protein Adsorption, ACS Appl. Mater. Interfaces. 8 (2016) 11819–11829. doi:10.1021/acsami.6b03107.

[5] Z. Sun, Y. Deng, J. Wei, D. Gu, B. Tu, D. Zhao, Hierarchically Ordered Macro-/Mesoporous Silica Monolith: Tuning Macropore Entrance Size for Size-Selective Adsorption of Proteins, Chem. Mater. 23 (2011) 2176–2184. doi:10.1021/cm103704s.

[6] L.L. Zhang, X.S. Zhao, Carbon-based materials as supercapacitor electrodes, Chem. Soc. Rev. 38 (2009) 2520. doi:10.1039/b813846j.

[7] D.-W. Wang, F. Li, H.-M. Cheng, Hierarchical porous nickel oxide and carbon as electrode materials for asymmetric supercapacitor, J. Power Sources. 185 (2008) 1563–1568. doi:10.1016/j.jpowsour.2008.08.032.

[8] K. Xia, Q. Gao, J. Jiang, J. Hu, Hierarchical porous carbons with controlled micropores and mesopores for supercapacitor electrode materials, Carbon N. Y. 46 (2008) 1718–1726. doi:10.1016/j.carbon.2008.07.018.

[9] D.-W. Wang, F. Li, M. Liu, G.Q. Lu, H.-M. Cheng, 3D Aperiodic Hierarchical Porous Graphitic Carbon Material for High-Rate Electrochemical Capacitive Energy Storage, Angew. Chemie Int. Ed. 47 (2008) 373–376. doi:10.1002/anie.200702721.

[10] S.J. Hollister, Porous scaffold design for tissue engineering, Nat. Mater. 4 (2005) 518–524. doi:10.1038/nmat1421.

[11] S.S. Liao, F.Z. Cui, W. Zhang, Q.L. Feng, Hierarchically biomimetic bone scaffold materials: Nano-HA/collagen/PLA composite, J. Biomed. Mater. Res. 69B (2004) 158–165. doi:10.1002/jbm.b.20035.

[12] J.R. Jones, P.D. Lee, L.L. Hench, Hierarchical porous materials for tissue engineering, Philos. Trans. R. Soc. London A Math. Phys. Eng. Sci. 364 (2006).

[13] J. Wei, J. Jia, F. Wu, S. Wei, H. Zhou, H. Zhang, J.-W. Shin, C. Liu, Hierarchically microporous/macroporous scaffold of magnesium–calcium phosphate for bone tissue regeneration, Biomaterials. 31 (2010) 1260–1269. doi:10.1016/j.biomaterials.2009.11.005.

[14] P. Koci, F. Stepanek, M. Kubicek, M. Marek, Modelling of micro/nano-scale concentration and temperature gradients in porous supported catalysts, Chem. Eng. Sci. 62 (2007) 5380–5385. doi:10.1016/j.ces.2006.12.033.

[15] P. Koci, V. Novak, F. Stepanek, M. Marek, M. Kubicek, Multi-scale modelling of reaction and transport in porous catalysts, Chem. Eng. Sci. 65 (2010) 412–419. doi:10.1016/j.ces.2009.06.068.

[16] R. Hill, Elastic properties of reinforced solids: Some theoretical principles, J. Mech. Phys. Solids. 11 (1963) 357–372. doi:10.1016/0022-5096(63)90036-X.

[17] M. Blunt, Flow in porous media—pore-network models and multiphase flow, Curr. Opin. Colloid Interface Sci. 6 (2001) 197–207. doi:10.1016/S1359-0294(01)00084-X.

[18] N. Hansen, R. Krishna, J.M. VanBaten, A.T. Bell, F.J. Keil, Analysis of diffusion limitation in the alkylation of benzene over H-ZSM-5 by combining quantum chemical calculations, molecular simulations, and a continuum approach, J. Phys. Chem. C. 113 (2009) 235–246. doi:10.1021/jp8073046.

[19] H. Li, M. Ye, Z. Liu, A multi-region model for reaction–diffusion process within a porous catalyst pellet, Chem. Eng. Sci. 147 (2016) 1–12. doi:10.1016/j.ces.2016.03.004.

[20] V. Novak, P. Koci, M. Marek, F. Stepanek, P. Blanco-Garcia, G. Jones, Multi-scale modelling and measurements of diffusion through porous catalytic coatings: An application to exhaust gas oxidation, Catal. Today. 188 (2012) 62–69. doi:10.1016/j.cattod.2012.03.049.

[21] M. Chabanon, B. David, B. Goyeau, Averaged model for momentum and dispersion in hierarchical porous media, Phys. Rev. E - Stat. Nonlinear, Soft Matter Phys. 92 (2015) 23201. doi:10.1103/PhysRevE.92.023201.

[22] J.H. Petropoulos, J.K. Petrou, A.I. Liapis, Network model investigation of gas transport in bidisperse porous adsorbents, Ind. Eng. Chem. Res. 30 (1991) 1281–1289. doi:10.1021/ie00054a031.

[23] J.J. Meyers, A.I. Liapis, Network modeling of the intraparticle convection and diffusion of molecules in porous particles packed in a chromatographic column, J. Chromatogr. A. 827 (1998) 197–213. doi:10.1016/S0021-9673(98)00658-X.

[24] J.J. Meyers, A.I. Liapis, Network modeling of the convective flow and diffusion of molecules adsorbing in monoliths and in porous particles packed in a chromatographic column, J. Chromatogr. A. 852 (1999) 3–23. doi:10.1016/S0021-9673(99)00443-4.

[25] A. Kaestner, E. Lehmann, M. Stampanoni, Imaging and image processing in porous media research, Adv. Water Resour. 31 (2008) 1174–1187. doi:10.1016/j.advwatres.2008.01.022.

[26] W.B. Lindquist, S.-M. Lee, D.A. Coker, K.W. Jones, P. Spanne, Medial axis analysis of void structure in three-dimensional tomographic images of porous media, J. Geophys. Res. Solid Earth. 101 (1996) 8297–8310. doi:10.1029/95JB03039.

[27] P. Spanne, J.F. Thovert, C.J. Jacquin, W.B. Lindquist, K.W. Jones, P.M. Adler,

Synchrotron Computed Microtomography of Porous Media: Topology and Transports, Phys. Rev. Lett. 73 (1994) 2001–2004. doi:10.1103/PhysRevLett.73.2001.

[28] W.B. Lindquist, A. Venkatarangan, Investigating 3D geometry of porous media from high resolution images, Phys. Chem. Earth, Part A Solid Earth Geod. 24 (1999) 593–599. doi:10.1016/S1464-1895(99)00085-X.

[29] H. Dong, M.J. Blunt, Pore-network extraction from micro-computerized-tomography images, Phys. Rev. E. 80 (2009) 36307. doi:10.1103/PhysRevE.80.036307.

[30] A.S. Al-Kharusi, M.J. Blunt, Network extraction from sandstone and carbonate pore space images, J. Pet. Sci. Eng. 56 (2007) 219–231. doi:10.1016/j.petrol.2006.09.003.

[31] A. Rabbani, S. Jamshidi, S. Salehi, An automated simple algorithm for realistic pore network extraction from micro-tomography images, J. Pet. Sci. Eng. 123 (2014) 164–171. doi:10.1016/j.petrol.2014.08.020.

[32] D. Silin, T. Patzek, Pore space morphology analysis using maximal inscribed spheres, Phys. A Stat. Mech. Its Appl. 371 (2006) 336–360. doi:10.1016/j.physa.2006.04.048.

[33] M.P. Hollewand, L.F. Gladden, Representation of porous catalysts using random pore networks, Chem. Eng. Sci. 47 (1992) 2757–2762.

[34] Z. Jiang, M.I.J. van Dijke, K. Wu, G.D. Couples, K.S. Sorbie, J. Ma, Stochastic Pore Network Generation from 3D Rock Images, Transp. Porous Media. 94 (2012) 571–593. doi:10.1007/s11242-011-9792-z.

[35] J.T. Gostick, M.A. Ioannidis, M.W. Fowler, M.D. Pritzker, Pore network modeling of fibrous gas diffusion layers for polymer electrolyte membrane fuel cells, J.

Power Sources. 173 (2007) 277–290. doi:10.1016/j.jpowsour.2007.04.059.

[36] R.D. Hazlett, Statistical characterization and stochastic modeling of pore networks in relation to fluid flow, Math. Geol. 29 (1997) 801–822. doi:10.1007/BF02768903.

[37] J. Gostick, M. Aghighi, J. Hinebaugh, T. Tranter, M.A. Hoeh, H. Day, B. Spellacy, M.H. Sharqawy, A. Bazylak, A. Burns, W. Lehnert, A. Putz, OpenPNM: A Pore Network Modeling Package, Comput. Sci. Eng. 18 (2016) 60–74. doi:10.1109/MCSE.2016.49.

[38] J.R. Welty, C.E. Wicks, G. Rorrer, R.E. Wilson, Fundamentals of momentum, heat, and mass transfer, John Wiley & Sons, 2009.

July 17th 2017

Dear reviewer,

Here is a list of highlights concerning the submitted manuscript:

- A general multiscale pore network reactive transport framework is proposed.
- A flexible multiscale network generation algorithm is presented.
- Guidelines are presented for designing high performance catalyst particles.
- Hierarchical particles with lower pore size ratio are generally more favorable.
- Influence of macroporosity in hierarchical particles is tightly linked with kinetics.

Thank you for considering this manuscript.

Sincerely,

Jeff Gostick